

Communication

# Adhesive Hybrid $\text{SiO}_{2.01}\text{C}_{0.23}\text{H}_x$ Nanoparticulate Coating on Polyethylene (PE) Separator by Roll-to-Roll Atmospheric Pressure Plasma

Yichao Jin <sup>1</sup>, Chaoliang Wang <sup>1,\*</sup>, Nana Yuan <sup>1</sup>, Ke Ding <sup>1</sup>, Yu Xu <sup>1</sup>, Sicheng Qin <sup>1</sup>, Ming Wang <sup>1</sup>, Zhuangchun Wu <sup>2</sup>, Chengran Du <sup>1</sup>, Jianjun Shi <sup>1</sup> and Jing Zhang <sup>1,3,\*</sup>

<sup>1</sup> Department of Physics, Donghua University (DHU), Shanghai 201600, China; 2161501@mail.dhu.edu.cn (Y.J.); 2171622@mail.dhu.edu.cn (N.Y.); dingke@dhu.edu.cn (K.D.); 1142024@mail.dhu.edu.cn (Y.X.); 2151400@mail.dhu.edu.cn (S.Q.); 2151414@mail.dhu.edu.cn (M.W.); chengran.du@dhu.edu.cn (C.D.); JShi@dhu.edu.cn (J.S.)

<sup>2</sup> Functional Materials Research Institute, Donghua University (DHU), Shanghai 201600, China; zwu@dhu.edu.cn

<sup>3</sup> Member of Magnetic Confinement Fusion Research Centre, Ministry of Education, Shanghai 201600, China

\* Correspondence: chaoliangwang@dhu.edu.cn (C.W.); jingzh@dhu.edu.cn (J.Z.); Tel.: +86-21-6779-2088 (J.Z.)

Received: 25 February 2019; Accepted: 12 March 2019; Published: 14 March 2019



**Abstract:** For the ever-increasing demand for highly safe lithium-ion batteries (LIBs), the common sol-gel process provides heat-resistance to separators with an inorganic coating, where the adhesion to the separator is the key to safety and stability. In this paper, we present a  $\text{SiO}_{2.01}\text{C}_{0.23}\text{H}_x$ -coated polyethylene (PE) separator through a roll-to-roll atmospheric plasma-enhanced chemical vapor deposition (R2R-APECVD) of hexamethyldisiloxane (HMDSO)/Ar/O<sub>2</sub>. The adhesion strength of  $\text{SiO}_{2.01}\text{C}_{0.23}\text{H}_x$ -coated PE was tested by peel-off test and found to be higher than that of the commercial Al<sub>2</sub>O<sub>3</sub>-coated separator (0.28 N/mm vs. 0.06 N/mm). Furthermore, the  $\text{SiO}_{2.01}\text{C}_{0.23}\text{H}_x$ -coated PE separator showed better electrochemical performance in C-rate and long term cycle tests. FTIR, SEM, and XPS analysis indicate that the increased adhesion and electrochemical performance are attributed to the inner hybrid  $\text{SiO}_{2.01}\text{C}_{0.23}\text{H}_x$  coating with organic and inorganic components.

**Keywords:** adhesion; hybrid nanoparticulate coating; atmospheric pressure plasma; chemical vapor deposition; lithium-ion battery separator

## 1. Introduction

Compared with lead-acid, nickel-cadmium, and nickel-hydrogen batteries, LIBs have the advantages of relatively high energy density, low pollution, and long lifespan, which have potential applications in electromobile and energy storage systems [1–4]. Extensive research efforts have been devoted to achieving the high energy density, enhanced C-rate, and superior safety features required to obtain short charging times and long driving distances for electric vehicles [5–8]. In addition to the development of novel and advanced electrodes and electrolytes, many studies have focused on improving the performance of separators [9–11].

In LIBs, the separator ensures electrical insulation and provides ion channels between the positive and negative electrodes [12]. It also provides safety through the closing of pores during thermal runaway. Coating separators with inorganic particles, such as Al<sub>2</sub>O<sub>3</sub>, SiO<sub>2</sub>, and TiO<sub>2</sub>, is a feasible and affordable way to achieve high-efficiency and -safety cells. However, the ordinary wet or sol-gel coating method usually causes problems in adhesion between the separators and the nanoparticles. Some of the coatings could detach from the separator surface and cause non-uniform impedance of the separator, which diminishes the electrochemical performance [13–16]. The performance of the coated separator

also affects the capacity and cycle performance of the LIBs directly [17,18]. In addition, wet coatings with a binder usually involve wet processes, which are relatively complicated and environmental unfriendly [19,20]. Chemical vapor deposition (CVD) of SiO<sub>2</sub> and atomic layer deposition (ALD) of Al<sub>2</sub>O<sub>3</sub> or TiO<sub>2</sub> are novel methods with promising performances using a dry process conducted in a vacuum chamber for the preparation of composite separators or electrodes [21–23]. However, it is necessary to seek out more eco-efficient separator coating manufacturing processes to ensure the safety of LIBS.

Recently, non-thermally reactive atmospheric pressure plasma has attracted much attention for its simplicity and flexibility as a dry method of film deposition [23–26]. Plasma is an ionized gas composed of positive charged ions, negative charged ions, electrons, and radicals which have high reactive energy [27,28]. It can provide a unique environment for chemical reactions and film growth, which is distinct from typical condensed chemical reactions driven by a single heat source. All the reactions occur at low gas temperature and far from chemical equilibrium. This method shows great potential in industrial applications for producing temperature-sensitive substrate coatings.

In our previous work, SiO<sub>x</sub>C<sub>y</sub>H<sub>z</sub> or TiO<sub>2</sub> nanoparticulate films have been successfully obtained by atmospheric pressure plasma-enhanced chemical vapor deposition (AP-PECVD) [29,30]. The purpose of this study is to investigate the structure and composition of the nanoparticulate coating and to obtain detailed information of the interfacial adhesion between the nanoparticulates coating and the PE separator by scanning electron microscopy (SEM), attenuated total reflection Fourier transform infrared spectroscopy (ATR-FTIR), X-ray photoelectron spectroscopy (XPS), and the peel-off test. There have been some studies that reported using atmospheric plasma to introduce hydrophilicity to the separator and increase Al<sub>2</sub>O<sub>3</sub> adhesion with the separator [31]. We fail to find similar reports of AP-PECVD of hybrid nanoparticulate coating with increased adhesion. Therefore, we used Al<sub>2</sub>O<sub>3</sub> coating as a comparison experiment. A noticeably improved adhesion strength was obtained and ascribed to the surface and inner SiO<sub>2.01</sub>C<sub>0.23</sub>H<sub>x</sub> nanoparticulate coating. A better cell performance of C-rate and cycling than that with Al<sub>2</sub>O<sub>3</sub> coating was achieved.

## 2. Materials and Methods

A commercial PE separator (12 μm thickness) was passed through the plasma zone at a controlled speed of 30 mm/min in a roll-to-roll way. The SiO<sub>x</sub>C<sub>y</sub>H<sub>z</sub> nanoparticulate coating on PE separator was directly achieved by modulating the hexamethyldisiloxane (HMDSO)/O<sub>2</sub>/Ar plasma system (flow rate in mL/min: 18/18/1600) for 3 min. Ar (99.990%) and O<sub>2</sub> (99.500%) was purchased from Shanghai Shenzhong Gas Co., Ltd (Shanghai, China). HMDSO was purchased from Merck-Schuchardt (Hohenbrunn, Germany). The plasma zone was 50 mm × 50 mm and generated by a discharge power source of 13 kHz and 10 W. Al<sub>2</sub>O<sub>3</sub> particle-coated PE (30 μm thickness; 5 μm coating layer:) was used for comparison. The commercial Al<sub>2</sub>O<sub>3</sub> particle-coated separator was purchased from Shenzhen Senior New Energy Material Co., Ltd (Shenzhen, China).

The adhesion strength between the coated layer and the PE separator was measured through the peel-off test: 3M adhesive tape with 19 mm wide and 90 mm long (Scotch 600, 3M Material Technology Co.,Ltd., Suzhou, China) was attached to the separator and then pressed on evenly with a metal roller of 2 kg. The sticky tape was detached by peeling at an angle of 180° with a constant displacement rate of 100 mm/min. In order to guarantee the reproducibility of the test, we conducted the test at least three times for each sample and calculated the average adhesion strength.

The chemical structure of the separators was measured by attenuated total reflectance Fourier-transform infrared spectroscopy (Nicolet 6700 at 4 cm<sup>-1</sup> spectral resolution, ThermoFisher Scientific, Waltham, MA, USA). The surface and cross-section morphologies were investigated by FE-SEM (S-4800, Hitachi, Tokyo, Japan). Qualitative analysis of the elemental composition of the membrane surface was analyzed by XPS (Escalab 250Xi, ThermoFisher Scientific, Waltham, MA, USA). In order to avoid the influence of the etching process or native layer of PE on the results, we performed the XPS test of the nanoparticles on quartz and 3-min-coated PE. We found that their XPS results are

close, so it is reasonably deduced that the oxide observed for silicon and carbon is not from the native surface layer. A cleaning sputtering was done before the tests to remove the surface layer of oxide.

Electrochemical properties were measured with coin-type  $\text{LiFePO}_4/\text{Li}$  half-cells (CR2032, Shenzhen Kejing Star Technology Co., Ltd, Shenzhen, China). Coin cells were assembled by sandwiching the separators between the lithium metal anode and  $\text{LiFePO}_4$  cathode. The cathode was prepared by casting a *N*-methyl-2-pyrrolidone (NMP)-based slurry ( $\text{LiFePO}_4$ :acetylene black: Polyvinylidene fluoride (PVDF) = 8:1:1 by weight) on aluminum foil (14  $\mu\text{m}$  thickness), followed by drying at 110  $^\circ\text{C}$  for 12 h under vacuum. Charge–discharge cycling tests of the lithium-ion cells were conducted at various C-rates over the voltage range from 2.5 to 4.2 V using a battery test system (LAND CT2001A).

### 3. Results and Discussions

#### 3.1. Morphological and Compositional Changes

The morphological and composition changes in the PE separators were characterized using FE-SEM, ATR-FTIR, and XPS. As shown in Figure 1a, the surface of the pristine PE consists of interlaced fibers and submicron pores, which is a typical morphology derived from wet processing. Figure 1b clearly shows that many nanoparticles were uniformly coated on the PE surface and closely interconnected on the fibers. We add two high magnification SEMs into Figure 1a,b (inset) for observing the pore and coated nanoparticles in detail. The particle sizes range from approximately 20 to 250 nm and the average diameter was 94.2 nm (Figure 1c).

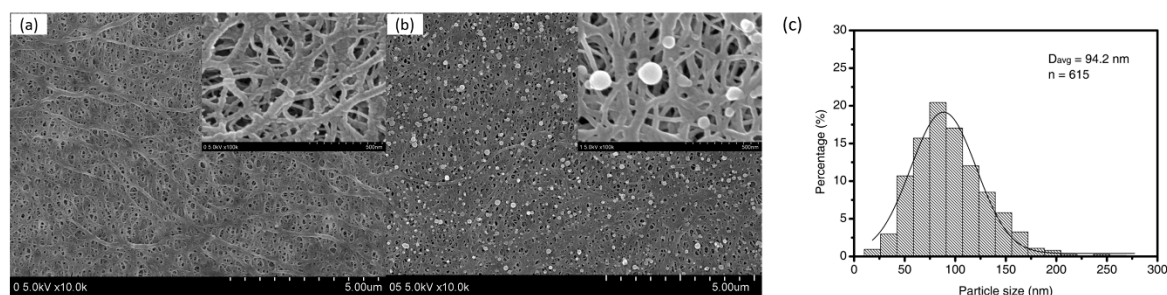


**Figure 1.** (a) Scanning electron microscopy (SEM) and high magnification (inset) images of bare polyethylene (PE); (b) SEM and high magnification (inset) images of the nanoparticle-coated PE separator; (c) size range of the nanoparticle on PE surface in (b).

Figure 2a shows the spectra of the untreated and plasma-coated PE through the ATR-FTIR. In the untreated PE separator, the strong bands at 2916 and 2849  $\text{cm}^{-1}$  are assigned to asymmetric and symmetric  $\text{CH}_2$  stretching vibrations, respectively. The peaks at 1471 and 714  $\text{cm}^{-1}$  are assigned to  $\text{CH}_2$  bending deformation and rocking deformation, respectively. After the deposition process, new Si-, C-, or O-based functional groups are present. The plasma-coated PE displays bands on 1077 and 930  $\text{cm}^{-1}$  corresponding to Si–O–Si asymmetric stretching vibrations and Si–OH stretching, respectively. The broad band from 3100–3700  $\text{cm}^{-1}$  is attributed to OH stretching in the Si–OH or C–OH groups [32]. These results confirm the successful introduction of functional groups like  $\text{SiO}_x$ ,  $\text{Si}(\text{CH}_3)_x$ , Si–OH, and C–OH into the PE separator.

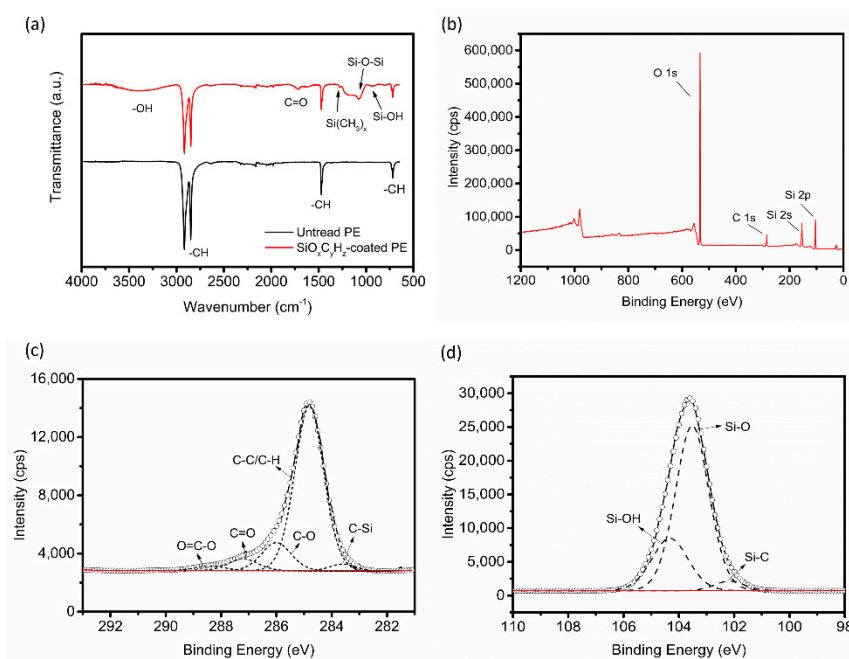


**Figure 2.** (a) Attenuated total reflection Fourier transform infrared spectroscopy (ATR-FTIR) spectra before and after plasma coating; (b) x-ray photoelectron spectroscopy (XPS) spectrum for the  $\text{SiO}_x\text{C}_y\text{H}_z$  nanoparticulate film; (c) C 1s spectra; (d) Si 2p spectra.

According to the XPS in Figure 2b, the formula of the nanoparticulate film on PE can be written as  $\text{SiO}_{2.01}\text{C}_{0.23}\text{H}_x$  (Si 2p: 30.8%, C 1s: 7.1%, O 1s: 62.1%). The fitted C 1s and Si 2p spectra are presented in Figure 2c,d and display inorganic bands of  $\text{SiO}_2$  and  $\text{SiO}_x$ , organic bands of C–O, C–C, and C=O, as well as a Si–C hybrid band. The percentage of the organic component (C–O, C–C, and C=O) and hybrid component (Si–C) according to the fitted C spectrum is 95% and 5%, respectively, while that of the inorganic and hybrid components in fitted Si 2p spectrum is 28% and 72%, respectively. Thus, it is reasonably deduced that the  $\text{SiO}_{2.01}\text{C}_{0.23}\text{H}_x$  nanoparticulate coating is mostly composed of inorganic components like  $\text{SiO}_2$  and small amount of organic components like C–O, C–C, and C=O, as well as hybrid structures like Si–C, which helps to improve the adhesion performance of the coating.

The nanoparticulate distribution on the cross-section of separators was identified using energy dispersive X-ray spectroscopy (EDS). As shown in Figure 3a, the plasma-coated film on PE is difficult to discern. However, the atomic percentage of Si and O are very high, near the surface of plasma-coated PE, and gradually decrease with depth into the center, confirming that the coating is thin and reaches into the inner fibers. As displayed in Figure 3d–f, there is a distinct boundary line between the  $\text{Al}_2\text{O}_3$  coating and the PE. The thickness of the  $\text{Al}_2\text{O}_3$  layer is about 5  $\mu\text{m}$ , and Al and O are concentrated on the PE surface.

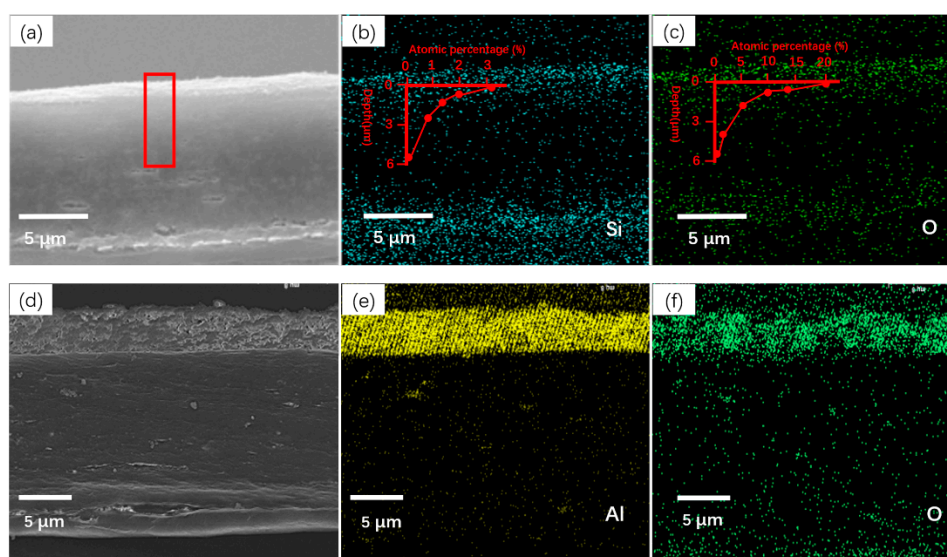


**Figure 3.** (a) Cross-section SEM image of  $\text{SiO}_{2.01}\text{C}_{0.23}\text{H}_x$ -coated PE separator; (b,c) are corresponding energy dispersive X-ray spectroscopy (EDS) maps of the Si and O, respectively; (d) cross-section SEM image of  $\text{Al}_2\text{O}_3$  particle-coated PE separator; (e,f) are corresponding EDS maps of the Al and O, respectively.

### 3.2. Adhesion Characteristics of the Coatings

The coating adhesion strength is closely related with the coating structure and composition. As analyzed from SEM, FTIR, and XPS, the coating is a layer of nanoparticulate film on top of and deep inside the PE separator. It is composed of inorganic components like  $\text{SiO}_2$ ,  $\text{SiO}$ , and  $\text{Si-OH}$ , and organic components like  $\text{C-O}$ ,  $\text{C-C}$ , or  $\text{C=O}$ , as well as hybrid components like  $\text{Si-C}$ , which connects the nanoparticulate layer closely to the PE separator and helps improve the adhesion performance of the coating with the organic separator. As displayed and discussion in Section 3.1 above, the hybrid  $\text{SiO}_{2.01}\text{C}_{0.23}\text{H}_x$  nanoparticulate coating is distributed across the porous separator cross-section in a gradient, which is benefit for improving the coating with the organic separator. Figure 4a shows that the bare tape does not have any discernible surface roughness. Figure 4d shows that micro  $\text{Al}_2\text{O}_3$  particles cover the separator densely, and no fiber network can be observed. The surface of the residual separators and the tapes after the peel-off test is shown in Figure 4b–f, respectively. Many uniformly distributed nanoparticles can still be clearly observed on the plasma-coated PE in Figure 4b. The SEM images of the tape surface removed from the plasma-coated PE shows few nanoparticles (Figure 4c). Because the striped nanoparticles had been affected by the surrounding glue, no sharp boundary of the particles can be clearly observed. These results indicate that the nanoparticulate layer was tightly bound to the PE surface. However, it can be seen in Figure 4e that most of the PE fiber network was exposed and only a few  $\text{Al}_2\text{O}_3$  particles remained on the PE separator after the peeling processing. The  $\text{Al}_2\text{O}_3$  particle layer was almost completely removed and stuck onto the tape (Figure 4f).

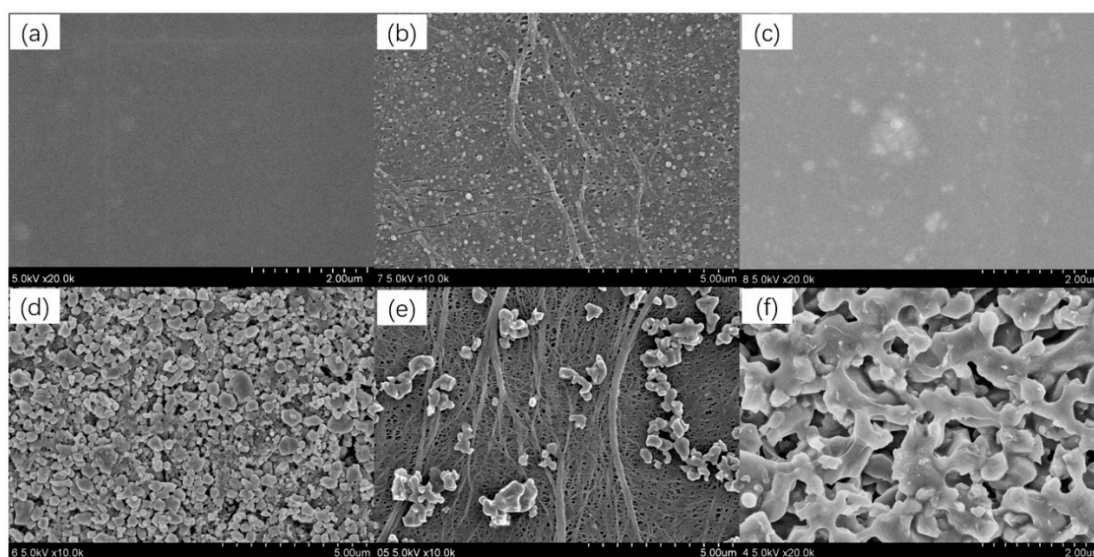


**Figure 4.** SEM images of (a) bare tape; (b) the  $\text{SiO}_{2.01}\text{C}_{0.23}\text{H}_x$ -coated PE separator after peel-off test; (c) corresponding tape surface to (b); (d) the  $\text{Al}_2\text{O}_3$  particle-coated PE separator; (e) the  $\text{Al}_2\text{O}_3$  particle-coated PE separator after peel-off test; (f) corresponding tape surface to (e).

As shown in Figure 5a, the  $\text{SiO}_{2.01}\text{C}_{0.23}\text{H}_x$ -nanoparticulate coated PE shows greatly improved adhesion strength (0.28 N/mm) compared with that of the  $\text{Al}_2\text{O}_3$  particle-coated PE (0.06 N/mm). The optical photo (Figure 5b) clearly shows that the tape peeling off from the plasma-coated PE remained transparent, whereas the tape from the  $\text{Al}_2\text{O}_3$  particle-coated PE became white with the  $\text{Al}_2\text{O}_3$  particle layer visible to the naked eye. Weighing the PE samples before and after peeling showed that the  $\text{Al}_2\text{O}_3$  particle-coated PE had a 12.58% weight loss, while the  $\text{SiO}_{2.01}\text{C}_{0.23}\text{H}_x$ -nanoparticulate-coated PE had almost zero weight loss. This indicates that  $\text{SiO}_{2.01}\text{C}_{0.23}\text{H}_x$ -nanoparticulate coating adheres to PE surface firmly; however, the adhesion measurement needs to improve because the application situation will not be the same as during a test.

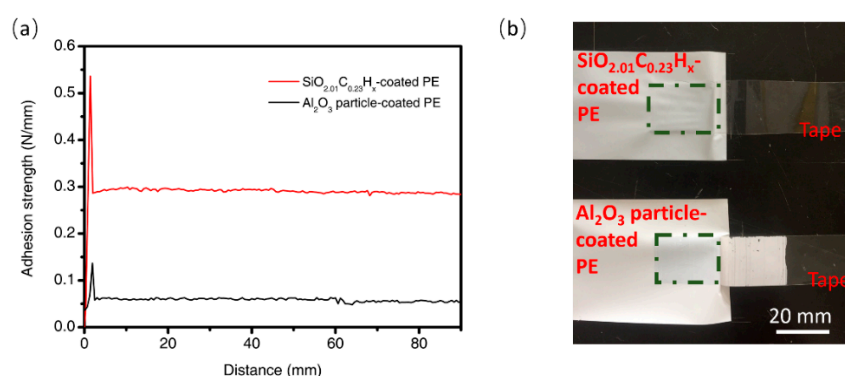


**Figure 5.** (a) Adhesion strengths of different coating samples; (b) the optical photo of the separators and tapes after the 180° peel-off test.

### 3.3. Electrochemical Performance

The cycling performances of cells assembled with the  $\text{Al}_2\text{O}_3$  particle-coated PE or  $\text{SiO}_{2.01}\text{C}_{0.23}\text{H}_x$ -coated PE was evaluated with a voltages ranged from 2.5 to 4.2 V at 0.5 C. As shown in Figure 6a, for the first cycle, the  $\text{SiO}_{2.01}\text{C}_{0.23}\text{H}_x$ -nanoparticulate-coated PE separator showed a discharge capacity of  $150.1 \text{ mA}\cdot\text{h}\cdot\text{g}^{-1}$  and a coulombic efficiency of 99.8%. In contrast, the  $\text{Al}_2\text{O}_3$  particle-coated PE separator had a discharge capacity of  $147.3 \text{ mA}\cdot\text{h}\cdot\text{g}^{-1}$  and a coulombic efficiency of 99.6%. After 200 cycles, the  $\text{SiO}_{2.01}\text{C}_{0.23}\text{H}_x$ -nanoparticulate-coated PE separator maintained

89.94% of its initial discharge capacity, which is higher than the  $\text{Al}_2\text{O}_3$  particle-coated PE separator, which maintained 83.1%.

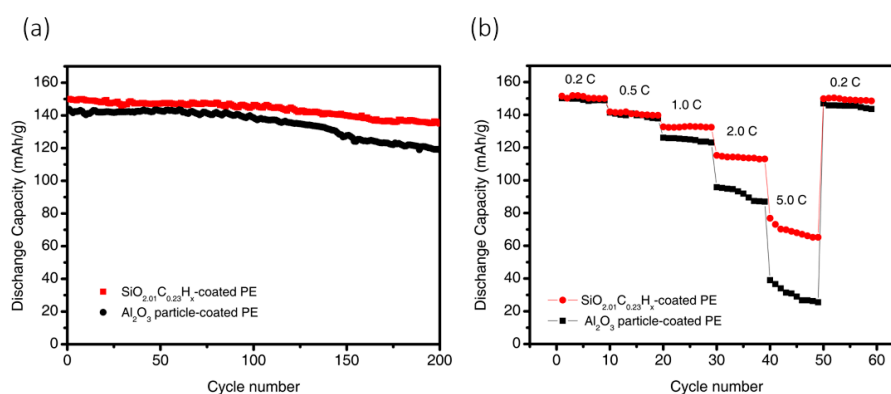


**Figure 6.** (a) The cycling performance; (b) C-rate capacity.

We evaluated the C-rate performance of the cells at discharge rates ranging from 0.2 to 5 C. As shown in Figure 6b, when the discharge rate is less than 1 C, the difference in the discharge capacity retention is negligible. This difference becomes obvious at 1 C. At a discharge rate of 5 C, the cell with the  $\text{SiO}_{2.01}\text{C}_{0.23}\text{H}_x$ -nanoparticulate-coated PE separator retained 45.6% of the initial discharge capacity of 0.1 C, while the  $\text{Al}_2\text{O}_3$  particle-coated PE separator retained only 20.6%. The deposition of the hybrid structure causes the coatings stick to the separator more tightly. Meanwhile, the reactive groups provide more ion channels during the charge and discharge process. It provides similar or even better electrochemical performance than that using atmospheric graft plasma or oxidization plasma.

#### 4. Conclusions

With focus on enhancing the adhesion between the PE separator and nanoparticulate coating, AP-PECVD was successfully used to deposit a hybrid  $\text{SiO}_{2.01}\text{C}_{0.23}\text{H}_x$  nanoparticulate layer on the top surface of and deep inside the PE separator. The atomic ratio of O/C and Si/C decreases from the top surface to the middle of the separator in a gradient. This nanoparticulate layer is composed of inorganic components like  $\text{SiO}_2$ , SiO, and Si-OH, and organic components like C-O, C-C, or C=O, as well as hybrid components like Si-C. This hybrid coating connects the nanoparticulate layer closely with PE separator and helps to improve the adhesion performance of the coating with the organic separator. The average adhesion strength of a plasma-coated separator is 0.28 N/mm, which is much higher than that of commercial  $\text{Al}_2\text{O}_3$  particle-coated separators (0.06 N/mm). Moreover, the cell with the  $\text{SiO}_{2.01}\text{C}_{0.23}\text{H}_x$ -coated separator delivered better electrochemical performance in C-rate and long-term cycle tests than that with a  $\text{Al}_2\text{O}_3$  particle-coated separator. In consequence, this simple but effective method could be proposed as a potential alternative to the conventional inorganic particle coating process.

**Author Contributions:** Conceptualization, J.Z. and C.W.; Methodology, J.Z.; Software, Y.J.; Validation, Y.J.; Formal Analysis, Y.J., C.W., S.Q., and M.W.; Investigation, Y.J., N.Y., K.D., S.Q., Y.X., J.S., C.D., and M.W.; Resources, J.Z. and Z.W.; Data Curation, Y.J.; Writing—Original Draft Preparation, Y.J.; Writing—Review and Editing, Y.J., C.W., and J.Z.; Visualization, Y.J.; Supervision, J.Z.; Project Administration, J.Z.; Funding Acquisition, J.Z.

**Funding:** This research was financially supported by the Fundamental Research Funds for the Central Universities and the Nature Science Foundation of China (Nos. 10835004, 11375042, 11475043 and 11875104).

**Acknowledgments:** We are grateful to Shanghai Energy New Materials Technology Co., Ltd. who provided the PE separator and Analysis and Testing Center of Donghua University who offered comprehensive materials testing services.

**Conflicts of Interest:** The authors declare no conflict of interest.

## References

1. Liu, M.-H.; Zhang, P.-P.; Gou, L.; Hou, Z.; Huang, B. Enhancement on the thermostability and wettability of lithium-ion batteries separator via surface chemical modification. *Mater. Lett.* **2017**, *208*, 98–101. [[CrossRef](#)]
2. Cui, Z.Y.; Shi, H.B.; Ding, J.Y.; Zhang, J.; Wang, H.; Wang, H. Fabrication of poly (vinylidene fluoride) separator with better thermostability and electrochemical performance for lithium ion battery by blending polyester. *Mater. Lett.* **2018**, *228*, 466–469. [[CrossRef](#)]
3. Chawla, N.; Bharti, N.; Singh, S. Recent advances in non-flammable electrolytes for safer lithium-ion batteries. *Batteries* **2019**, *5*, 19. [[CrossRef](#)]
4. Zhang, K.; Xiao, W.; Liu, J.; Yan, C. A novel self-binding composite separator based on poly(tetrafluoroethylene) coating for Li-ion batteries. *Polymers* **2018**, *10*, 1409. [[CrossRef](#)]
5. Zhao, J.; Hu, Q.; Wang, J.; Zhang, P.; Zhu, Y.; Wu, G.; Lv, Y.; Lv, L.; Zhao, Y.; Yang, M. Effects of island-coated PVdF-HFP composite separator on the performance of commercial lithium-ion batteries. *Coatings* **2018**, *8*, 437. [[CrossRef](#)]
6. Shi, C.; Dai, J.; Li, C.; Shen, X.; Peng, L.; Zhang, P.; Wu, D.; Sun, D.; Zhao, J. A modified ceramic-coating separator with high-temperature stability for lithium-ion battery. *Polymers* **2017**, *9*, 159. [[CrossRef](#)]
7. Lee, H.W.; Muralidharan, P.; Ruffo, R.; Mari, C.M.; Cui, Y.; Kim, D.K. Ultrathin spinel  $\text{LiMn}_2\text{O}_4$  nanowires as high power cathode materials for Li-ion batteries. *Nano Lett.* **2010**, *10*, 3852. [[CrossRef](#)]
8. Wang, G.; Liu, H.; Liu, J.; Qiao, S.; Lu, G.M.; Munroe, P.; Ahn, H. Mesoporous  $\text{LiFePO}_4/\text{C}$  nanocomposite cathode materials for high power lithium ion batteries with superior performance. *Adv. Mater.* **2010**, *22*, 4944. [[CrossRef](#)]
9. Kritzer, P.; Döring, H.; Emermacher, B. Improved safety for automotive lithium batteries: An innovative approach to include an emergency cooling element. *Adv. Chem. Eng. Sci.* **2014**, *4*, 197–207. [[CrossRef](#)]
10. Zhu, W.; Huang, X.; Liu, T.; Xie, Z.; Wang, Y.; Tian, K.; Bu, L.; Wang, H.; Gao, L.; Zhao, J. Ultrathin  $\text{Al}_2\text{O}_3$  coating on  $\text{LiNi}_{0.8}\text{Co}_{0.1}\text{Mn}_{0.1}\text{O}_2$  cathode material for enhanced cycleability at extended voltage ranges. *Coatings* **2019**, *9*, 92. [[CrossRef](#)]
11. Lee, H.; Yanilmaz, M.; Toprakci, O.; Fu, K.; Zhang, X. A review of recent developments in membrane separators for rechargeable lithium-ion batteries. *Energy Environ. Sci.* **2014**, *7*, 3857. [[CrossRef](#)]
12. Linden, D.; Reddy, T.B. *Handbook of Batteries*; McGraw-Hill: New York, NY, USA, 2002.
13. Arora, P.; Zhang, Z. Battery separators. *Chem. Rev.* **2004**, *104*, 4419–4462. [[CrossRef](#)] [[PubMed](#)]
14. Zhang, S.S. A review on the separators of liquid electrolyte Li-ion batteries. *J. Power Sources* **2007**, *164*, 351–364. [[CrossRef](#)]
15. Tobishima, S.-I.; Yamaki, J.-I. A consideration of lithium cell safety. *J. Power Sources* **1999**, *81*, 882–886. [[CrossRef](#)]
16. Lee, H.; Jeon, H.; Gong, S.; Ryou, M.-H.; Yong, M.-L. A facile method to enhance the uniformity and adhesion properties of water-based ceramic coating layers on hydrophobic polyethylene separators. *Appl. Surf. Sci.* **2018**, *427*, 139–146. [[CrossRef](#)]
17. Cai, M.; Zhu, J.; Yang, C.; Gao, R.; Shi, C.; Zhao, J. A parallel bicomponent TPU/PI membrane with mechanical strength enhanced isotropic interfaces used as polymer electrolyte for lithium-ion battery. *Polymers* **2019**, *11*, 185. [[CrossRef](#)]
18. Liu, J.C.; Yang, K.; Mo, Y.D.; Wang, S.J.; Han, D.M.; Xiao, M.; Meng, Y.Z. Highly safe lithium-ion batteries: High strength separator from polyformaldehyde/cellulose nanofibers blend. *J. Power Sources* **2018**, *400*, 502–510. [[CrossRef](#)]
19. Starostin, S.A.; Premkumar, P.A.; Creatore, M.; de Vries, H.; Paffen, R.M.J.; van de Sanden, M.C.M. High current diffuse dielectric barrier discharge in atmospheric pressure air for the deposition of thin silica-like films. *Appl. Phys. Lett.* **2010**, *96*, 061502. [[CrossRef](#)]
20. Alf, M.E.; Asatekin, A.; Barr, M.C.; Baxamusa, S.H.; Chelawat, H.; Ozaydin-Ince, G.; Petruczok, C.D.; Sreenivasan, R.; Tenhaeff, W.E.; Trujillo, N.J.; et al. Chemical vapor deposition of conformal, functional, and responsive polymer films. *Adv. Mater.* **2010**, *22*, 1993–2027. [[CrossRef](#)]
21. Ma, D.; Li, Y.; Yang, J.; Mi, H.; Luo, S.; Deng, L.; Yan, C.; Zhang, P.; Lin, Z.; Ren, X.; et al. Robust  $\text{SnO}_{2-x}$  nanoparticle-impregnated carbon nanofibers with outstanding electrochemical performance for advanced sodium-ion batteries. *Nano Energy* **2018**, *43*, 317. [[CrossRef](#)]
22. Gawlik, G.; Ciepiewski, P.; Baranowski, J.M. Study of implantation defects in CVD graphene by optical and electrical methods. *Appl. Sci.* **2019**, *9*, 544. [[CrossRef](#)]

23. Hu, Z.; Zheng, D.; Tu, R.; Yang, M.; Li, Q.; Han, M.; Zhang, S.; Zhang, L.; Goto, T. Structural controlling of highly-oriented polycrystal 3C-SiC bulks via halide CVD. *Materials* **2019**, *12*, 390. [[CrossRef](#)] [[PubMed](#)]
24. Jäger, E.; Schmidt, J.; Pfuch, A.; Spang, S.; Beie, O.; Jäger, N.; Jantschner, O.; Daniel, R.; Mitterer, C. Antibacterial silicon oxide thin films doped with zinc and copper grown by atmospheric pressure plasma chemical vapor deposition. *Nanomaterials* **2019**, *9*, 255. [[CrossRef](#)] [[PubMed](#)]
25. Sun, C.; Min, J.; Lin, J.; Wan, H. Effect of atmospheric pressure plasma treatment on adhesive bonding of carbon fiber reinforced polymer. *Polymers* **2019**, *11*, 139. [[CrossRef](#)]
26. Zhang, J.; Di, L.; Yu, F.; Duan, D.; Zhang, X. Atmospheric-pressure cold plasma activating Au/P<sub>25</sub> for CO oxidation: effect of working gas. *Nanomaterials* **2018**, *8*, 742. [[CrossRef](#)] [[PubMed](#)]
27. Dudina, D.V.; Bokhonov, B.B.; Olevsky, E.A. Fabrication of porous materials by spark plasma sintering: A review. *Materials* **2019**, *12*, 541. [[CrossRef](#)]
28. Kaushik, N.K.; Kaushik, N.; Linh, N.N.; Ghimire, B.; Pengkit, A.; Sornsakdanuphap, J.; Lee, S.-J.; Choi, E.H. Plasma and nanomaterials: fabrication and biomedical applications. *Nanomaterials* **2019**, *9*, 98. [[CrossRef](#)] [[PubMed](#)]
29. Qin, S.; Wang, M.; Wang, C.; Jin, Y.; Yuan, N.; Wu, Z.; Zhang, J. Binder-free nanoparticulate coating of a polyethylene separator via a reactive atmospheric pressure plasma for lithium-ion batteries with improved performances. *Adv. Mater. Interfaces* **2018**, *5*, 1800579. [[CrossRef](#)]
30. Wang, D.; Yang, Q.; Guo, Y.; Liu, X.; Shi, J.; Zhang, J. One step growth of TiO<sub>2</sub> crystal trees by atmospheric pressure plasma jet. *Mater. Lett.* **2011**, *65*, 2526–2529. [[CrossRef](#)]
31. Jeon, H.; Jin, S.; Park, W.; Lee, H.; Kim, H.; Ryou, M.; Lee, Y. Plasma-assisted water-based Al<sub>2</sub>O<sub>3</sub> ceramic coating for polyethylene-based microporous separators for lithium metalsecondary batteries. *Electrochim. Acta* **2016**, *212*, 649–656. [[CrossRef](#)]
32. Wang, Z.; Zhu, H.; Yang, L.; Wang, X.; Liu, Z.; Chen, Q. Plasma modified polypropylene membranes as the lithium-ion battery separators. *Plasma Sci. Technol.* **2016**, *18*, 424. [[CrossRef](#)]



© 2019 by the authors. Licensee MDPI, Basel, Switzerland. This article is an open access article distributed under the terms and conditions of the Creative Commons Attribution (CC BY) license (<http://creativecommons.org/licenses/by/4.0/>).